Boundary-Layer Meteorol (2013) 147:165–178
DOI 10.1007/s10546-012-9774-x

ARTICLE

Fine-Scale Characteristics of Temperature, Wind, and Turbulence in the Lower Atmosphere (0–1,300 m) Over the South Peruvian Coast

Ben B. Balsley · Dale A. Lawrence · Ronald F. Woodman · David C. Fritts

Received: 13 February 2012 / Accepted: 19 September 2012 / Published online: 12 October 2012

Abstract We report results of preliminary high-resolution in situ atmospheric measurements through the boundary layer and lower atmosphere over the southern coast of Perú. This region of the coast is of particular interest because it lies adjacent to the northern coastal edge of the sub-tropical south-eastern Pacific, a very large area of ocean having a persistent stratus deck located just below the marine boundary layer (MBL) inversion. Typically, the boundary layer in this region during winter is topped by a quasi-permanent, well-defined, and very large temperature gradient. The data presented herein examine fine-scale details of the coastal atmosphere at a point where the edge of this MBL extends over the coastline as a result of persistent onshore flow. Atmospheric data were gathered using a recently-developed in-house constructed, GPS-controlled, micro-autonomous-vehicle aircraft (the DataHawk). Measured quantities include high-resolution profiles of temperature, wind, and turbulence structure from the surface to 1,300 m.

Keywords Coastal boundary layer · Fine-scale measurements · In situ measurements · Marine boundary layer · Mini-autonomous vehicles · Turbulence profiles

B. B. Balsley (✉)
Cooperative Institute for Research in Environment Sciences, University of Colorado, Boulder, CO, USA
e-mail: balsley@cires.colorado.edu

D. A. Lawrence
Aerospace Engineering Department, University of Colorado, Boulder, CO, USA

R. F. Woodman
Instituto Geofísico del Perú, Lima, Peru

D. C. Fritts
GATS, Boulder, CO, USA

1 Introduction

The need to better understand atmospheric dynamics on scales as small as metres and seconds has been justified in a series of recent observations (Cho et al. 2003; Ström and Tjernström 2003; Balsley et al. 2008; Tjernström et al. 2009). It is also supported by recent results using direct numerical simulation (DNS) modelling (Fritts et al. 2009). Stated briefly, both observations and modelling results show that the criteria for atmospheric instability are strongly scale dependent, with the criteria being met much more often as scale size decreases. Thus, although the atmosphere may appear statically and dynamically stable when examined on vertical scales of a hundred metres or more, smaller-scale temperature and velocity gradients arising from a combination of pre-existing low-level, small-scale turbulence, linear or non-linear gravity waves, and similar factors can significantly enhance the unstable nature of the atmosphere at these smaller scales (see comments in Tjernström et al. 2009, Fritts et al. 2009, and Fernando and Weil 2010).

Fine-scale studies of the marine boundary layer (MBL) and its overland counterpart near the coast are of considerable interest, particularly in view of the effects of the interactions between these two regions on local weather conditions, pollution transport, and larger-scale climate variations (Riordan et al. 1985; McElroy and Smith 1991; Holt 1996; Grisogono et al. 1998; Edwards et al. 2001; Ström and Tjernström 2003; Angevine et al. 2006).

The results presented herein are based on a brief initial campaign designed to examine the fine-scale dynamics of the atmosphere along the southern Peruvian coast using an in-house designed mini-autonomous-vehicle (MAV) called the DataHawk. This particular region was selected for two reasons: (1) the anomalously strong, and semi-permanent inversion at the top of the boundary layer near the coast provided an excellent opportunity for coastal boundary-layer studies, including the inversion, and (2) owing to the paucity of low-altitude aircraft activity in the area, limitations on unmanned aircraft flights were much less restrictive compared to restrictions at more populated sites.

In this paper we describe measurements in this region obtained by the DataHawk, documenting details of the edge of the MBL as it is advected a few kilometres inland by the local onshore breeze. Specifically, we document details of temperature, wind, and fine-scale turbulence from the surface up to 1,300 m, i.e., to heights well above the top of the MBL as it extends over the coast. These initial results focus on the post-sunrise period, when the local winds are relatively weak and the onshore breezes are light but steady. Future, more extended, campaigns are underway to include the entire early morning period, from prior to sunrise until the strong winds begin late morning (see Sect. 3).

We begin with brief descriptions of MBL characteristics in the near-coastal sub-tropical south-eastern Pacific (SEP) (Sect. 2), followed by a description of the campaign field site, including local weather conditions (Sect. 3), and salient details of the DataHawk MAV (Sect. 4). Subsequent sections discuss the campaign itself (Sect. 5), present the data analyses (Sect. 6), and end with a discussion and conclusions (Sect. 7).

2 Overview of the Near-Coastal MBL in the South-Eastern Pacific Region

In the sub-tropical SEP, the combination of sustained south-westerly surface winds and the resulting upwelling of the cold waters of the Humboldt current give rise to a cold, moisture-laden MBL. Concomitant strong solar heating and subsidence of the sub-tropical troposphere, coupled with the cold, moist MBL, result in a strong and relatively steep temperature inversion at the top of the MBL. The magnitude of this inversion (5–15 °C) prevents boundary-layer

air from rising into the free atmosphere. The additional effect of onshore breezes produced by solar heating of the coastal desert transports this cold, moist MBL air a few kilometres inland, until the onshore flow is blocked by the nearby lofty Andean Cordillera to the east (see, e.g., Garreaud and Muñoz 2005).

The SEP region has been intensively studied during the recent Variability of the American Monsoon System (VAMOS) Ocean-Cloud Atmosphere-Land Study (VOCALS) (Rahn and Garreaud 2010). VOCALS took place during October–November 2008 and documented, among other things, the spatial and temporal variations of MBL height and magnitude between 14° and 25°S latitude (Rahn and Garreaud 2010). These authors reported that the mean MBL height extends to about 1,500 m some 1,500–1,600 km off the coast, decreasing systematically to about 1,100 m (±350 m) near the coast. The inversion magnitude, on the other hand, increases from ≈8 °C near the westernmost extent of this region, to ≈11 °C some 500 km from the coast. Closer to the coast, the inversion magnitude again decreases to ≈7 ± 4 °C.

Garreaud and Muñoz (2004) and Rahn and Garreaud (2010) also report on the diurnal variability of the MBL. Very near the coast, the MBL appears to be displaced upward during daytime and downward after local sunset. In addition, they point out the presence of a so-called 'upsidence' (in contrast to a *subsidence*) wave, which is apparently generated near the south Peruvian coast during the early evening hours, and which appears to modulate the diurnal variability of the MBL depth (Garreaud and Muñoz 2004, 2005). Vertical velocities slightly above the inversion near the coast exhibit magnitudes in excess of 0.01 m s^{-1} (upward and downward) on occasion, with maximum upward velocities occurring in late afternoon and maximum downward velocities occurring prior to local midnight.

3 Description of the Campaign Site

The DataHawk launch site at 13°55′43.2″S, 76°15′03.6″W was situated roughly 10 km south of Paracas, Perú in the *Reserva Nacional de Paracas*. A map of the region is provided in Fig. 1, and shows the near-linear character of the coastline south-west (roughly upwind) of the Reserva, running roughly from the north-west to the south-east. The area around the launch site (indeed, the entire southern Peruvian coast) is essentially an arid sandy desert, almost entirely devoid of vegetation. The launch site, indicated by an 'X' in Fig. 1, was situated 3–4 km inland at an altitude of 173 m above m.s.l., An expanded view of the launch area (lower right-hand corner of Fig. 1) shows the launch site situated at the bottom of a small depression surrounded by small (a few hundred m high) hills on the north-eastern to southern edge, and in the north-western quadrant. The horizons to the south-west and north were only slightly elevated.

One favorable feature of this portion of the Peruvian coast for MAV activities lies with the predictable surface wind pattern. This statement is illustrated in Fig. 2a, b, which present results of an analysis of the 15-min averaged diurnal wind speed magnitude for July 2000 (Fig. 2a), along with the 6-h averaged wind rose for July–August–September 2001 (Fig. 2b). Note that the wind rose only shows wind directions for the 0900–1299 local time (LT) period, i.e., around the observing period. Figure 2a is a plot of the probability of wind speeds greater than four nominal values (3, 5, 8, and 11 m s^{-1}) versus time. Examination of this figure shows that, between 0000 LT and 1000 LT, surface wind speeds are virtually always <5 m s^{-1}, with wind speeds >3 m s^{-1} occurring only about 20% of the time. Wind speeds increase systematically during late morning and early afternoon hours, maximizing between 1400–1900 LT, and subsequently decreasing to less than 3 m s^{-1} around 2000 LT. The wind rose in Fig. 2b

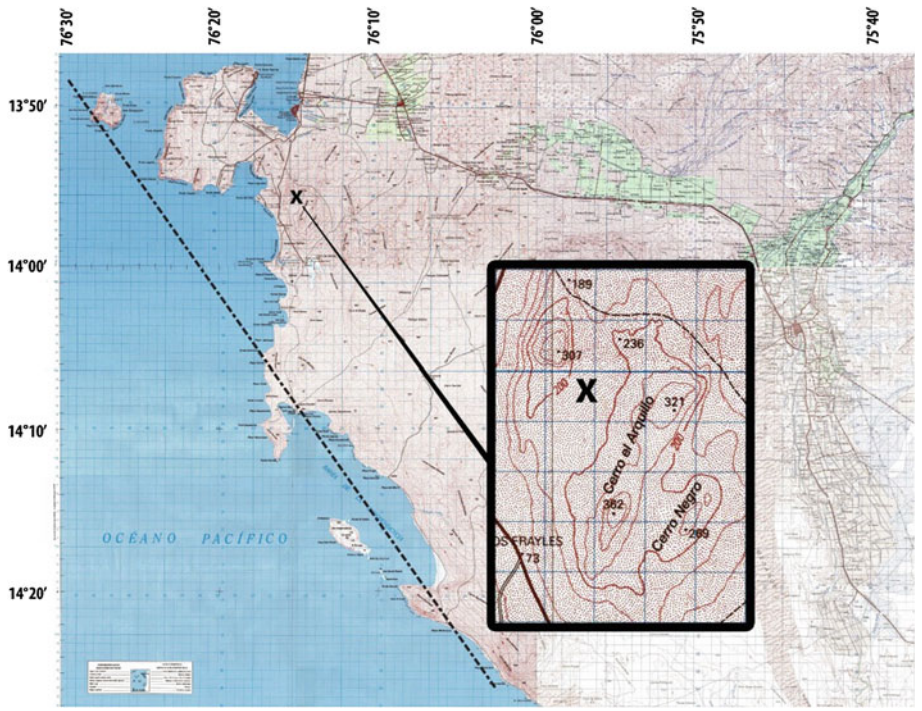

Fig. 1 Map of the south Peruvian coast from about 13°45′S to 14°25′S latitude. The DataHawk launch site is indicated by an '*X*' near the coast at the *top* of the figure. Latitude is indicated to the *left* of the figure. The *dashed black line* extending from the north-west to the south-east illustrates the nearly linear coastline lying approximately upwind of the launch site; the expanded view of the actual launch site shown in the *lower right-hand quadrant* shows 50-m contours of the surrounding topography

shows that the wind directions between 0900–1200 LT lie predominantly between southerly and north-westerly. The absence of any north-easterly wind component documents the lack of offshore breezes during that portion of the day, thus enabling a study of MBL evolution as the MBL is advected onshore.

The Paracas region is attractive for our studies for a number of other reasons. First, day-to-day weather conditions are very predictable and benign. Seasonal conditions are also predictable, with winter air temperatures being some 5 °C less than those in summer. Seasonal variations of sea-surface temperatures result in clear skies in summer and cloudy skies in winter, with (as mentioned earlier) a stratiform cloud deck lying below the inversion in winter (Wang et al. 2011). A second advantage for this campaign is that the Paracas launch site is reasonably remote from a number of interfering factors (traffic, heavy population density and radio frequency interference (e. g., WiFi)). Finally, it is important to point out that, since regional air traffic is minimal below 1,500 m, and international traffic is virtually non-existent below 9,000 m, flight permission for our flight activities was easily obtained from Peruvian authorities via the Corporación Peruana de Aeropuertos y Aviación Comercial (CORPAC).

Thus, in view of the fact that the SEP serves as a natural laboratory for studying the coupled ocean-atmosphere-land system (Rahn and Garreaud 2010), the southern Peruvian coastal region provides an ideal natural laboratory for high-resolution atmospheric studies at

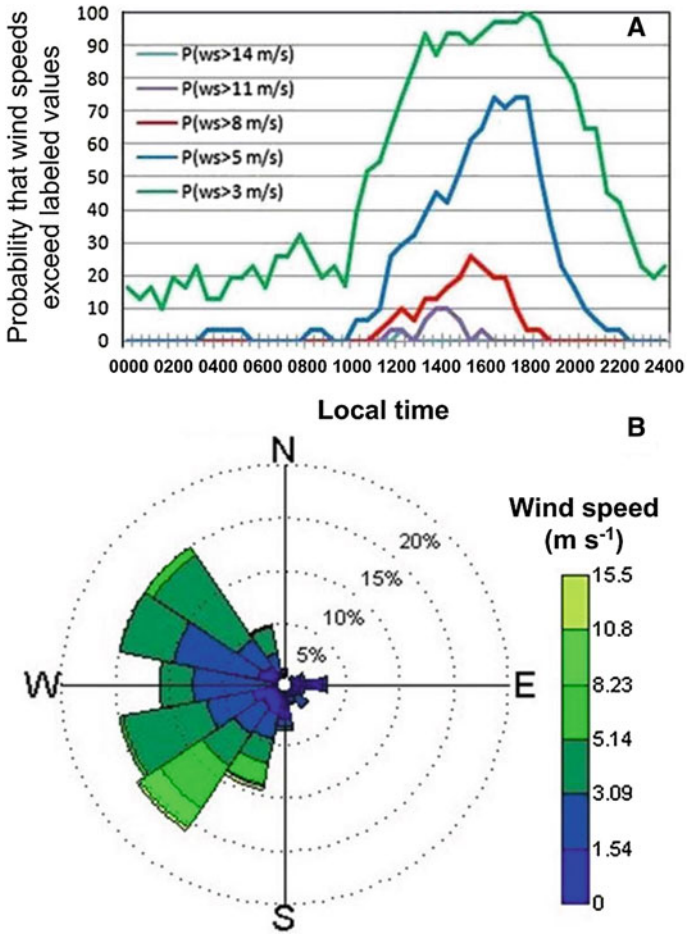

Fig. 2 **a** A plot of the results of a statistical analysis of 15-min averaged surface wind speed in the Paracas region. The four *curves* represent the probability that wind speeds are >3, 5, 8, and 11 m s^{-1}; **b** a wind rose for the Paracas region for July–September 2001 for the period 0900–1200 LT, i.e., near the flight times presented here

the interfacial coastal region adjacent to the SEP. Specific advantages include the presence of the steep MBL temperature inversion, the day-to-day predictability of the wind vector, the relatively benign climate, and the remoteness of the area from air traffic.

4 A Brief Description of the Datahawk (MAV) Vehicle

The DataHawk (Fig. 3) is a small, low-cost, programmable, reusable, autonomous, GPS-controlled, vehicle equipped with temperature, pressure, and humidity sensors, in addition to a 100-Hz cold-wire temperature probe for estimating turbulence via the temperature structure constant, C_T^2 (Lawrence and Balsley 2012). The aircraft is battery-powered and can gather high-resolution (∼1 m) atmospheric data from the surface up to 2–3 km height. The DataHawk was developed by the University of Colorado's

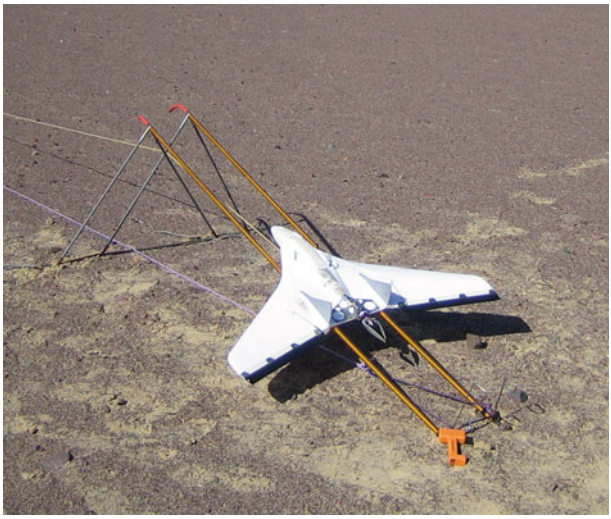

Fig. 3 Photograph of the 1-m wing span DataHawk ready to be launched by a bungee technique. The nearby *footprints* provide a rough idea of the small size of the aircraft

Aerospace Engineering Sciences Department (Allred et al. 2007; Pisano et al. 2007; Lawrence et al. 2008) and has been instrumented for high-resolution in-situ atmospheric measurements by that group in cooperation with University of Colorado's Cooperative Institute for Environmental Research (CIRES). Typical flight patterns involve an autonomous spiral ascent and descent. The spiral radius is adjustable in flight from 40 m to over 1 km, and the climb rate is also adjustable between ± 5 m s^{-1}. Thus, the vehicle can be also commanded to fly a series of constant altitude circles at various heights.

Take-offs and landings are autonomous, with take-offs typically achieved via a bungee launch. Because of the DataHawk's rugged Styrofoam fuselage, light weight, and relatively low airspeed (12–14 m s^{-1}), landings can be made virtually anywhere. All atmospheric data, GPS information, and other housekeeping details are telemetered to a ground-based receiver and data archiving system using a 2.4-GHz radio link. With the exception of the 100-Hz cold-wire data, all data are archived at 10 Hz. This information is available online at the ground station terminals for both monitoring and control purposes.

5 Campaign Overview

The results described in the following section were obtained during a brief two-day campaign on 16–17 July, 2011. Wind conditions, temperatures, and cloud cover during this period were similar to those described in Sect. 3 above. We present results from two separate DataHawk flights that began at 0811 LT and 0902 LT on 17 July 2011. The first flight consisted of a steady spiral ascent with a 50-m circle diameter, from the surface to 1,300 m, followed by a comparable descent. In contrast, the second flight involved flying a sequence of four separate constant-altitude circles over a 22-min period. The height sequence of these constant-height circles was 34, 43, 33, and 22 m. During this flight, the circle diameter was varied from 120 to 320 m.

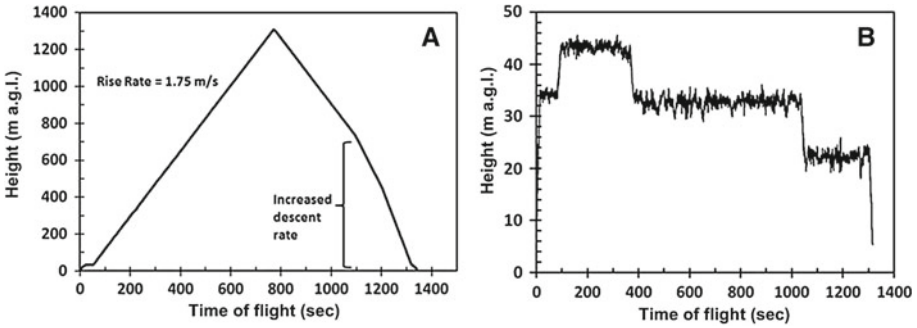

Fig. 4 Height versus time representation of the two flights described herein. Time is shown in seconds from the beginning of each flight: **a** illustrates the vertical pattern for the 0811 LT flight on 17 July 2011. The ascent rate was 0.75 m s^{-1}; the descent rate also began at 1.75 m s^{-1} but was increased to 3 m s^{-1} toward the last half of the descent. The horizontal flight pattern during this entire period was a helix with a radius of 50 m. In contrast, **b** the flight beginning 0902 LT on 17 July 2011 shows a series of constant altitude flights between 22 and 44 m. Constant-height circle diameters in this case were varied between 50 and 300 m

Height versus time plots of both flights are shown in Fig. 4a, b; the abscissae on both plots are scaled in seconds after launch. Note the constant (1.75 m s^{-1}) ascent and descent rates in Fig. 4a, until the DataHawk had descended to about 720 m, at which time the descent rate was increased to 3 m s^{-1}. Fig. 4b illustrates the constant altitude circle sequences and the ±2 m altitude maintenance during these circles. Nominal ascent/descent rate between the constant-altitude periods during the 0902 LT flight was ≈1.8 m s^{-1}.

6 Data Presentation

6.1 Temperature Profiles

Two temperature profiles using 10-Hz thermistor data obtained during both the 0811 LT ascent and descent are shown in Fig. 5. Both profiles have been smoothed by a 100-point (10-s) running average for convenience in viewing average trends. The height range covers zero to 1,300 m, and the time interval between launch and landing is roughly 22 min. Examination of Fig. 5 shows a number of notable similarities and differences between the two profiles:

- The near-surface temperatures were relatively unchanged during the 22-min flight.
- A slight temperature increase (0.5 °C) is apparent below the inversion.
- Both the height of the steep inversion between 600 and 760 m above ground level (a.g.l.) and the inversion magnitude (≈9 °C), were relatively unchanged between ascent and descent
- Above the inversion the temperature was relatively unchanged.

6.2 Wind Profiles

If the DataHawk flew a constant-altitude circular path in the absence of wind, a plot of GPS ground speed versus GPS heading would be a straight line. In other words, the ground speed would be independent of the direction of flight. In the presence of a constant horizontal wind, however, the ground speed would be less/more than the no-wind case when the aircraft

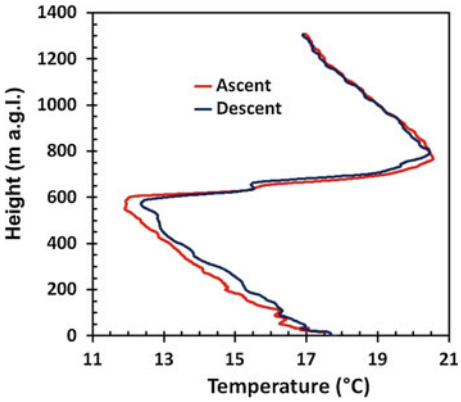

Fig. 5 Vertical profiles of temperature obtained during the ascent (*red*) and descent (*blue*) portions of 0811 LT flight. Note the slight (0.5 °C) warming below the inversion, and the relatively unchanged temperatures above 750 m. The height of the steep inversion appears unchanged during the 22-min flight. Both the magnitude (10 °C) and the height (600–760 m) of the inversion are consistent with those reported by Rahn and Garreaud (2010) for coastal MBL characteristics

would fly upwind/downwind. The maximum difference in either case would be equal to the magnitude of the wind, and the heading at which the ground speed was a minimum would indicate the wind direction. In the absence of other factors, the shape of this GPS ground speed versus GPS direction plot would be sinusoidal. In addition, the mean value of this sinusoid would represent the airspeed of the aircraft. Thus, the wind vector at aircraft altitude and the aircraft airspeed can be estimated by the shape of the GPS ground speed versus GPS heading plot.

To demonstrate these points, Fig. 6a shows an actual plot of GPS ground speed versus GPS direction (red) obtained when the DataHawk was ascending through a height interval of relatively constant wind speed around 650 m at 0811 LT on 17 July 2011. A second (black) theoretical sinusoidal curve has been added. This curve was produced by assuming that the DataHawk was ascending through a height range containing a constant 4.75 m s^{-1} wind coming from an azimuth of 150°. The close correspondence between these two curves clearly shows that the mean wind vector over this circular path was approximately that of the assumed value.

This same procedure can be used to produce a reasonable estimate of the wind-speed profile throughout the entire height range, provided we assume a constant aircraft velocity and a slowly changing wind pattern with height. In practice it is possible to use a quarter of a complete 360° curve for this determination. The use of quarter-circle portions has two advantages: first, the height resolution of the resulting wind profile is increased by a factor of four; second, the use of quarter-circle values reduces the potential errors when making wind vector estimates in the presence of a vertical wind shear.

Figure 6b shows the wind profile (speed and direction) for the 0811 LT ascent, estimated from quarter-circle portions of the GPS ground speed versus GPS direction data. Based on this figure, the character of the wind field between the surface and 1,300 m can be summarized as follows: the wind speeds throughout the entire height range were relatively low (3–4 m s^{-1}), with the exception of somewhat weaker winds in a narrow region just below the temperature inversion. Similarly, the general wind direction was southerly to south-easterly, except just below the inversion where the wind was easterly. Note that the near-surface wind direction in Fig. 6b is more southerly than the average direction indication on the wind rose in Fig. 2b.

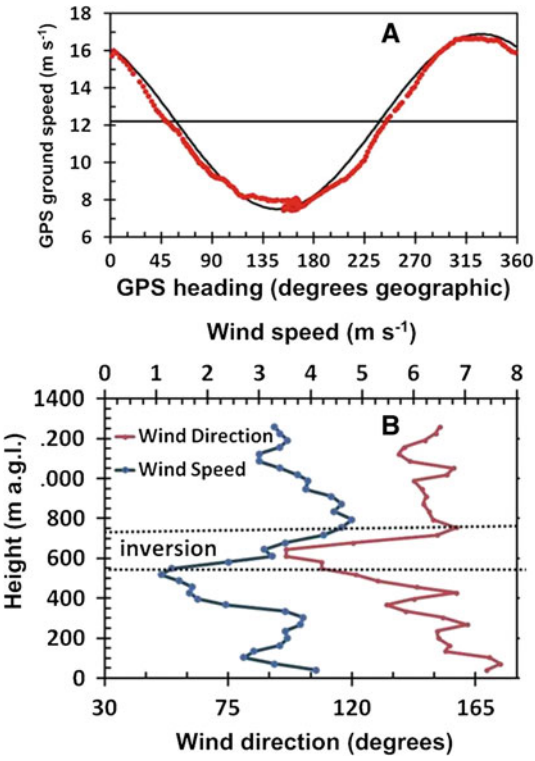

Fig. 6 **a** Plot of the observed GPS ground speed versus GPS heading (*red*) for a single circle at a height of 750 m obtained during the 0811 LT ascent. The included theoretical (*solid black*) curve would be that expected if the DataHawk were flying a constant altitude circle in the presence of a 4.75 m s^{-1} wind from an azimuth of 150°. The close agreement between these two curves demonstrates that this technique provides reasonable results for estimating the local wind vector. **b** The wind profile deduced for the entire 0811 LT ascent using the 26 technique described in (**a**). The primary difference in this profile relative to the **a** estimate is that the **b** profile was obtained using quarter-circle segments (90° portions) to estimate the wind vector to improve the vertical resolution of the profile

6.3 Temperature Fluctuations in the Steep Gradient Region

Figure 7 is a plot of cold-wire probe temperature fluctuations (red) associated with the ascent profile shown in Fig. 5. Figure 7 also includes the smoothed temperature profile (grey) from Fig. 5 for the region near the steep temperature gradient (500–750 m) for reference. The temperature fluctuations were obtained by subtracting 10-s smoothed temperature values from the non-smoothed cold-wire temperature data and then smoothing the results by 10 points (1 s). Both horizontal scales are plotted in °C, while the ordinate is the altitude (m.a.g.l.).

The temperature fluctuations shown in Fig. 7 (bottom scale) appear to be associated with the steep gradient region, and have a maximum peak-to-peak amplitude of 1 °C and a vertical wavelength of around 16 m. The maximum fluctuations occur around 620 m.

6.4 C_T^2 Turbulence Profile

A profile of the temperature turbulence structure constant C_T^2 for the ascent portion of the 0811 LT flight is presented in Fig. 8. Examination of this profile shows a number of distinct features. First, the turbulence magnitude is largest close to the surface, with surface values of C_T^2 approaching 0.1 $m^{-2/3}$ K^2. Turbulence magnitudes above the surface decrease systematically with height, decreasing by roughly three orders of magnitude before reaching a minimum around 550 m, i.e., slightly below the beginning of the steep inversion. The variability of C_T^2 with height in this lowest height range is appreciable, with that variability diminishing with increasing height. The height range containing the inversion (600–750 m)

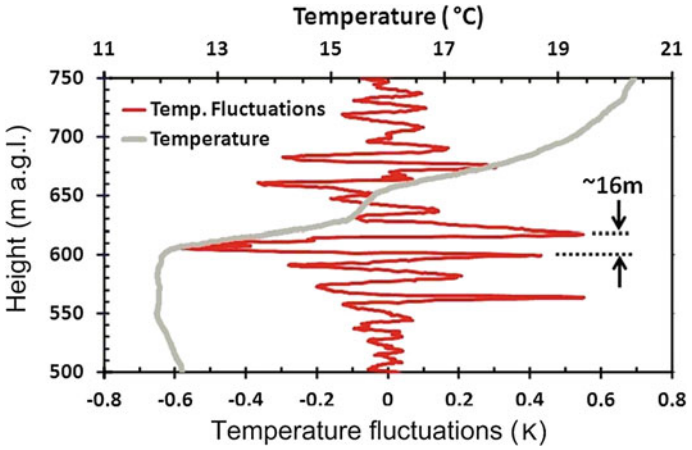

Fig. 7 Detailed view of the temperature profile in the steep gradient region between 500–750 m (*grey*) during the ascent portion of the flight shown in Fig. 5. Superimposed on the smoothed temperature plot is a plot of the temperature fluctuations (*red*), obtained by subtracting high-resolution cold-wire temperature values from their 100-point running mean. The results shown have been smoothed by an additional 10-point running mean. The resulting quasi-sinusoidal fluctuations have an apparent vertical wavelength of 16 m and a maximum peak to-peak amplitude of 1.0 °C

exhibits a relatively large increase in turbulence intensity by well over an order of magnitude, and contains significant order-of-magnitude variations. Above the top of the inversion, turbulence intensity decreases gradually with height, reaching a relatively constant value of $\approx 1 \times 10^{-4} \mathrm{m}^{-2/3}$ K^2. Above the inversion height, the variability of turbulent intensity with height is minimal.

6.5 Quasi-Coherent Temperature Structures

An intriguing characteristic of the high-resolution cold-wire temperature measurements observed when flying a large-diameter constant-altitude circle appears in Fig. 9 (a portion of the 0902 LT flight). In this instance the DataHawk flew in a 320-m diameter circle at an altitude of 34 m.a.g.l. Figure 9 is a plot of unsmoothed 10-Hz cold-wire temperature values as a function of time as the aircraft flew along the 1,000 m flight path around a single circle. The temperature values shown on the vertical scale range from 17 to 19.7 °C. Examination of Fig. 9 shows a series of quasi-coherent regions of enhanced temperature structures having relatively steep 'edges'. The region marked '∼200 m' identifies one such region. Three additional similar regions can be identified in this figure. The steepness of the edges of the enhancements can exceed 0.3 K m^{-1}. These enhancements have amplitudes that exceed 1 °C and contain sharp temperature 'peaks' as narrow as 7 m (e.g., the peak marked '∼7m').

7 Discussion and Conclusions

This campaign was intended primarily as a 'proof-of-concept' effort to document the capabilities of the DataHawk for the gathering of high-resolution atmospheric data. The results presented here demonstrate this capability. Although many of the DataHawk's sampling capabilities are evolving, the system as currently configured provides a useful low-cost (∼$1,000)

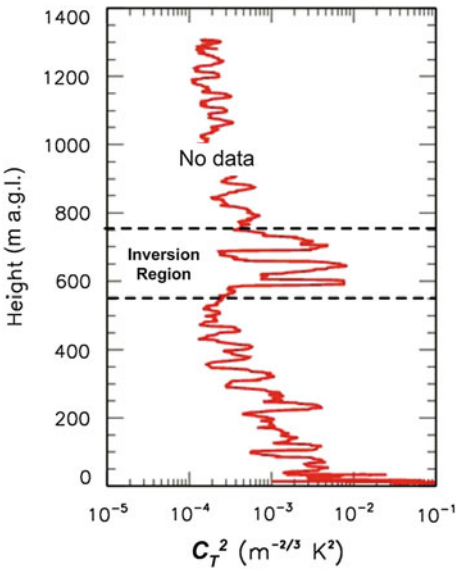

Fig. 8 Vertical profile of C_T^2 for the 0811 LT ascent. This profile has been smoothed by a 3-point running average of 3-s power spectra (a vertical smoothing of 17 m). Note the more than three orders of magnitude variability of C_T^2 over the height range, as well as the enhanced structured region just below the inversion

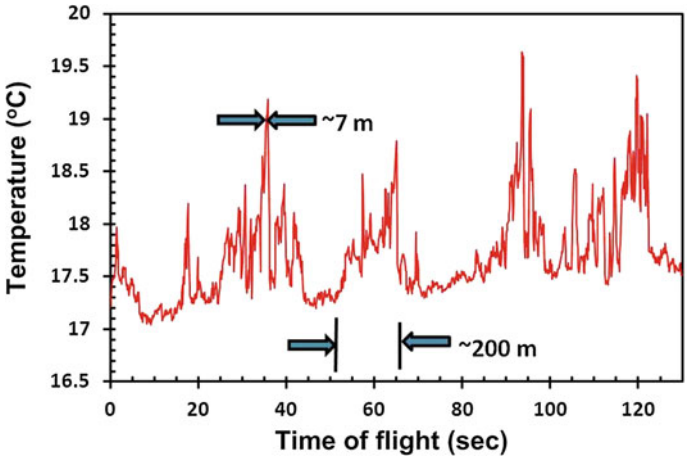

Fig. 9 Illustration of quasi-coherent temperature structure observed while flying a constant height circle at an altitude of 34 m. The radius of the circle was 320 m, so that the DataHawk flew along a circular 1-km path. The abscissa in this case 27 has been scaled in time of flight in seconds relative to the beginning of the circle. Note the occurrence of four such structures along the path (e.g., the region marked '∼200 m'), the enhanced sharp 'peaks' within these regions that can be a narrow as 7 m, and the abrupt 'sides' exhibited on the structures themselves

measurement capability that could be exploited more fully in future boundary-layer studies (Lawrence and Balsley 2012). The results included here provide an interesting insight into several intriguing aspects of the lower atmosphere over the south coast of Perú. Although it would be unreasonable to make any generalizations based on this limited dataset, it is reasonable to summarize the results as follows.

- The strong steep inversion atop the MBL is observable over the launch site, with the height, magnitude, and steepness associated with this feature as it approaches coast.

Thus, at least under winter conditions, the MBL over the SEP appears to encroach at least a few km inland, owing to the persistent onshore component of the south-westerly flow. Understanding of the ramifications of this encroachment may be aided by the coastline south of Paracas, which lies along an almost linear north-west to south-east line.

- At least on one occasion during the campaign, the inversion appeared to be associated with vertically-structured, quasi-sinusoidal, temperature fluctuations. The $\pm 0.5\,^{\circ}\mathrm{C}$ maximum fluctuation levels occurred near the inversion height, the vertical wavelength was close to 16 m, with the magnitude of the fluctuations decreasing significantly 100 m or so above and below the inversion. The source and ubiquity of this feature, its horizontal extent and stationarity, and other important characteristics remain to be delineated.
- The C_T^2 turbulence profile exhibited a number of features, some of which have commonality with observations elsewhere, and one of which is relatively unique. Common features include, (1) the intense near-surface turbulence levels that decreased significantly with increasing height up to the inversion height, and (2) the approximate constancy of the smaller turbulence intensities in the free atmosphere above the inversion. One unique feature of the C_T^2 profile is the greatly enhanced turbulence levels just below the inversion. Whether these enhanced levels are directly associated with non-linear interactions related to the quasi-coherent temperature fluctuations in this same height range remains to be established. It is worth pointing out that a number of authors (Lilly 1968; Blaskovic et al. 1991; Garreaud and Muñoz 2004; Angevine et al. 2006) have discussed the need to better understand the possible effects of enhanced turbulence on inversion heights.
- Results obtained during a constant-altitude flight showed the presence of quasi-coherent temperature enhancements along the flight path. These enhanced regions had elevated temperatures $> 1\,^{\circ}\mathrm{C}$ relative to their environment and contained large temperature fluctuations within the regions. Horizontal dimensions ranged from 7 m to more than 200 m, with sharp edges where the horizontal temperature gradients exceeded 0.3 K m^{-1}. Whether these features might conceivably be associated with early-morning convective plumes or with large-scale intermittent turbulence structures, much more work is needed to firmly establish such an association. It is worthwhile pointing out that these enhancements were virtually non-existent above the inversion.
- The constancy of the seasonal weather and surface wind patterns, coupled with the presence of the encroaching MBL over the area, provide an excellent and relatively uncomplicated venue for coastal boundary-layer studies. The interface between the MBL and its inland counterpart, and the complicating effects of this interface on pollution dispersion and local weather conditions, as well as on longer-scale climate variations, could be easily documented in this region of the coast, particularly in view of the nearly straight coastline upwind of the region.

Finally, the potential of incorporating DataHawk-like aircraft in future coastal boundary-layer studies (preferably with, or even without, additional atmospheric documentation from lidars, radars, instrumented towers, etc.) can be broadly categorized as follows:

(i) Individual DataHawks could measure vertical profiles of the lower atmosphere from either land or from ships. If the ship were located only a few km off the coast, ship-borne launches with land-based landings could be easily achieved. For locations farther from the coast, the aircraft could be returned to this ship and 'captured' using existing technology.

(ii) Individual DataHawks could also be used for constant-altitude flights between two locations separated by a few km. For example, it would be relatively easy to measure the horizontal variability of atmospheric quantities with the aircraft flying perpendicular

to the coastline, i.e., an on-land launch with the flight path extending a few km over the water and returning to land at a coastal site. Similarly, such flights could be made over hills upwind of the launch site to examine potential orographic effects that could modulate local coastal atmospheric dynamics.

(iii) It is feasible to consider including additional lightweight instruments for measuring aerosols or other trace variables for simultaneous sampling with existing onboard instruments.

(iv) Finally, given a number of DataHawks flying in a prescribed formation it would be reasonable to consider obtaining simultaneous high-resolution data within a three-dimensional volume containing the steep MBL inversion. Such a volume could be as large as several km, or as small as a few hundred metres, on a side.

Acknowledgements We are pleased to acknowledge significant assistance during the campaign portion of this effort by personnel of the Jicamarca Radio Observatory (JRO) near Lima, Perú. In particular, we appreciate the on-site help of Percy Condor (JRO), who also provided the statistics of the local Paracas winds. Appreciation is also extended to the Corporación Peruana de Aeropuertos Comercial (CORPAC) for providing permission to fly the DataHawk in the area. The late Dr. R. Frehlich and Dr. Y. Meillier of the University of Colorado's Cooperative Institute for Research in Environmental Sciences (CIRES) provided a number of useful comments and suggestions during the analysis portion of this project. Finally, we are happy to acknowledge the useful contributions of J. Rush (CIRES) during many phases of this project. This research was partially supported by the Army Research Office under ARO Contract W911NF-10-C-0109, the National Science Foundation under Award # AGS 1041963, in addition to an Innovative Research Proposal (IRP) awarded by CIRES.

References

Allred J, Hasan A, Panichsaku S, Pisano W, Gray P, Huang J, Han R, Lawrence D, Mohseni K (2007) Sensor flock: an airborne wireless sensor network of micro-air Vehicles. In: Proceedings of the ACM Sensys Conference, Sydney, ACM 1-59593-763

Angevine W, Hare J, Fairall C, Wolfe D, Hill R, Brewer W, White A (2006) Structure and formation of the highly stable marine boundary layer over the Gulf of Maine. J Geophys Res 111:D23S22. doi:10.1029/2006JD007465

Balsley B, Svensson G, Tjernström M (2008) On the scale-dependence of the gradient Richardson number in the residual layer. Boundary-Layer Meteorol 127:57–72

Blaskovic M, Davies R, Snider J (1991) Diurnal variation of marine stratocumulus over San Nicolas Island during July 1987. Mon Weather Rev 119:1469–1478

Cho J, Newell R, Anderson B, Barrick J, Thornhill K (2003) Characterizations of tropospheric turbulence and stability layers from aircraft observations. J Geophys Res 108:8784. doi:10.1029/2002JD002820

Edwards K, Rogerson A, Winan C, Rogers D (2001) Adjustment of the marine atmospheric boundary layer to a coastal cape. J Atmos Sci 58:1511–1528

Fernando H, Weil J (2010) Whither the stable boundary? Bull Am Meteorol Soc 91:1475–1484

Fritts D, Wang L, Werne J (2009) Gravity wave–fine structure interactions: a reservoir of small-scale and large-scale turbulence energy. Geophys Res Lett 36:L19805. doi:10.1029/2009GI039501

Garreaud R, Muñoz R (2004) The diurnal cycle in circulation and cloudiness over the Subtropical Southeast Pacific: a modeling study. J Clim 17:1699–1710

Garreaud R, Muñoz R (2005) The low-level jet off the west coast of subtropical South America: structure and variability. Mon Weather Rev 133:2246–2261

Grisogono B, Strom L, Tjernström M (1998) Small-scale variability in the coastal atmospheric boundary layer. Boundary-Layer Meteorol 88:23–46

Holt T (1996) Mesoscale forcing of a boundary layer jet along the California coast. J Geophys Res 101: 4235–4254

Lawrence D, Balsley B (2012) High-resolution atmospheric sensing using a low-cost miniature autonomous aerial vechicle. J Atmos Oceanic Technol (submitted)
Lawrence D, Frew E, Pisano W (2008) Lyapunov vector fields for autonomous UAV flight control. AIAA J Guid Control Dyn 31:1220–1229
Lilly D (1968) Models of cloud-topped mixed layers under a strong inversion. Q J R Meteorol Soc 94:292–309
McElroy J, Smith T (1991) Lidar descriptions of mixing-layer thickness characteristics in a complex terrain/coastal environment. J Appl Meteorol 30:585–597
Pisano W, Lawrence D, Gray P (2007) Autonomous UAV control using a 3-sensor autopilot. In: Proceedings of the AIAA Infotech@Aerosapce Conference, Rohnert Park, AIAA, pp 2007–2756
Rahn D, Garreaud R (2010) Marine boundary layer over the sub-tropical Pacific during VOCALS-Rex-Part 1: mean structure and diurnal cycle. Atmos Chem Phys 10:4491–4506
Riordan A, Sethraman S, Davis J, Viessman S (1985) Measurements of the marine boundary layer near a coastal front. Geophys Res Lett 12:681–684
Ström L, Tjernström M (2003) Variability in the summertime coastal marine boundary layer off California, USA. Q J R Meteorol Soc 130:423–448
Tjernströ̃m M, Balsley B, Svensson G, Nappo C (2009) The effects of critical layers on residual layer turbulence. J Atmos Sci 66:468–480
Wang L, Wang K, Lauer A, Xie S (2011) Simulation of seasonal variation of marine boundary layer clouds over the eastern Pacific with a regional climate model. J Clim 24:3190–3210